Supporting Information

Long-life and Deeply Rechargeable Aqueous Zn Anodes Enabled by Multifunctional Brightener-Inspired Interphase

Zhiming Zhao, Jingwen Zhao*, Zhenglin Hu, Jiedong Li, JiaJia Li, Yaojian Zhang, Cheng Wang and Guanglei Cui*

1. Experimental Details

Chemicals: Zinc trifluoromethanesulfonate ($Zn(TfO)_2$), Zinc sulfate ($ZnSO_4$), manganese sulfate ($MnSO_4$), anhydrous HCOOH, were purchased from Sigma-Aldrich. Zn plates (130 μm in thickness), Zn foils (20 μm in thickness), Ti foils, Nylon 6 non-woven fabrics, polyacrylonitrile (PAN, Mw = 150,000), polyethylene oxide (PEO, Mw = 600,000) were purchased from Qingdao Blue Sea & Delight Empire Co., Ltd. MnO_2 was prepared according to the method in the previous report.[1] PAN and PEO were dissolved in *N*, *N*-Dimethylformamide (DMF). The solutions were cast onto the electrode and then dried, and the thickness of the cating layer was 40 μm.

Characterization: Corrosion test and cyclic voltammetry were carried on an electrochemical workstation (VMP-300, Bio-Logic Science Instruments Co.). Linear polarization and chronoamperograms (CAs) measurements was conducted in a three-electrode configuration, in which bare Zn and coated Zn plate were used as the working respectively, Zn plate as the counter, and saturated calomel (SCE) as the reference electrodes. The corrosion potential and corrosion current were calculated from Tafel fit system in electrochemical workstation. EIS spectra were recorded on the electrochemical workstation with a frequency range from 7 MHz to 0.01 Hz.

Galvanostatic charge-discharge measurements were performed with a LAND CT2001A Battery Cycler (Wuhan, China).

Ionic conductivities were tested by two blocking electrodes (SS) and calculated according to the following equation:

$$\sigma = \frac{l}{R_b \cdot S} \qquad \text{Equation (S1)}$$

where R_b represents the resistance according to EIS measurement, l represents the thickness of the membrane, and S is the area of the contact between SS and electrolyte.

Zn^{2+} transference number were evaluated in symmetrical Zn battery combined by EIS before and after the CA test, and calculated by the following equation:

$$T = \frac{I_s(\Delta V - I_0 R_0)}{I_0(\Delta V - I_s R_s)} \qquad \text{Equation (S2)}$$

where ΔV is the voltage polarization applied, I_s and R_s are the steady state current and resistance, respectively, I_0 and R_0 are the initial current and resistance, respectively. Applied voltage polarization here in 5 mV.

Storage modulus, loss modulus, and viscosity measurement of the precursor solutions were done using a parallel-plate rheometer (ARES-G2, TA Instrument) at 25 °C. Dynamic mechanical analysis was performed on a DMA242 machine (NETZSCH) in tensile mode with a temperature increment of 3 °C min^{-1}. Water flux tests were performed by a dead-end filtration cell without adscititious pressure. The water flux J_w (L $(m^2 \cdot h)^{-1}$) was calculated by the following equation:

$$J_w = \frac{V}{A \cdot \Delta T} \qquad \text{Equation (S3)}$$

where V (L) was the volume of permeated water, A (m^2) was the membrane area and ΔT (h) was the permeation time. Oxygen permeability coefficient was conducted on

oxygen transmission rate test system (Labthink). DSC measurements were tested from −80 to 250 °C at 10 °C min^{-1} (TA Instruments, Q5000IR).

Transmission Fourier transform infrared spectroscopy (FTIR) spectra were carried out using EO-SXB IR spectrometer. Raman spectroscopy spectra were carried out using RENISHAWSYS1000 Raman spectrometer. The resolution is 4 cm^{-1}. The differential electrochemical mass spectrometry (DEMS) experiments were done with an ECC-Air cell (EL-CELL GmbH, Germany)

2. Supplementary Figures and Discussions

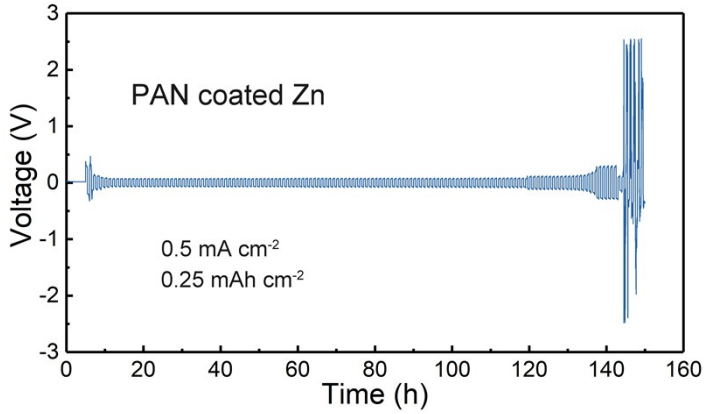

Fig. S1 Cycling performance of symmetrical Zn cells with PAN-coated Zn plates.

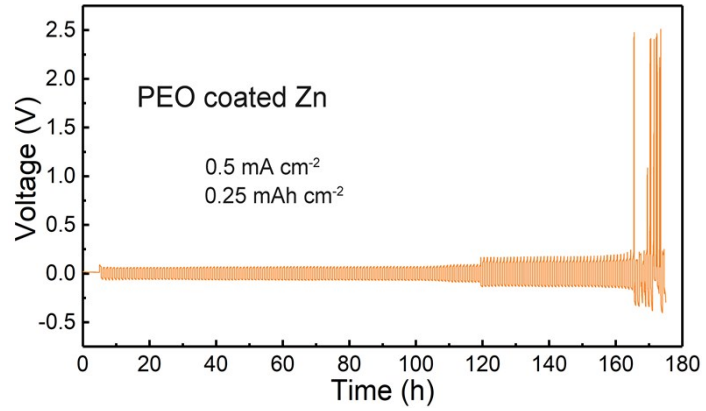

Fig. S2 Cycling performance of symmetrical Zn cells with PEO-coated Zn plates.

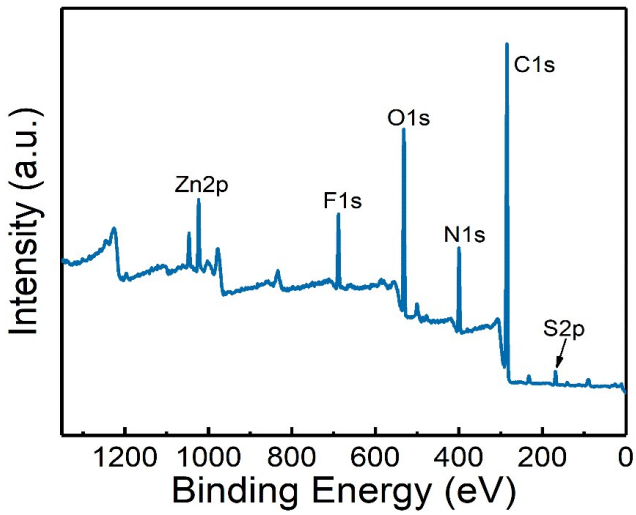

Fig. S3 XPS spectrum of the PA layer.

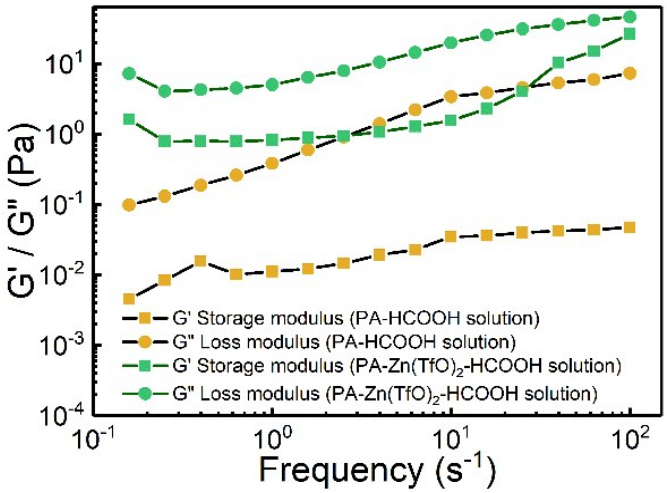

Fig. S4 Rheological study of HCOOH-dissolved PA solutions with and without $Zn(TfO)_2$.

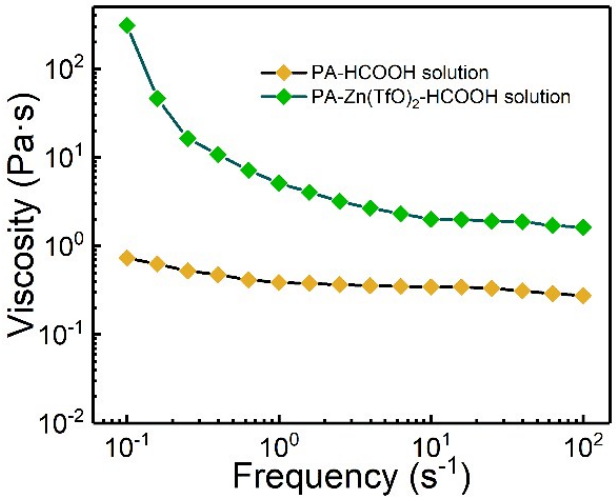

Fig. S5 Dynamic viscosity tests of HCOOH-dissolved PA solutions with and without $Zn(TfO)_2$.

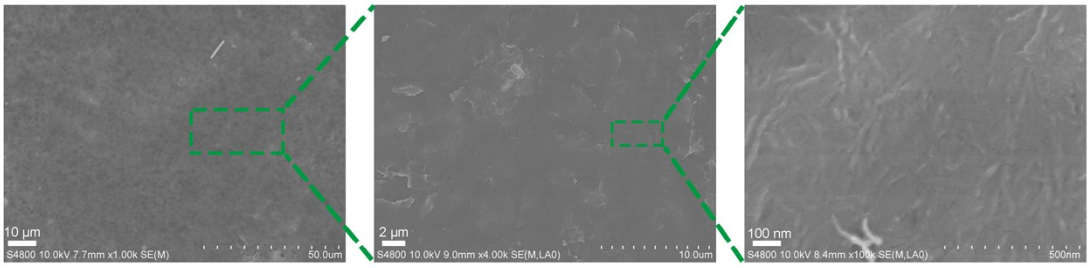

Fig. S6 The morphology of the PA layer with various magnification.

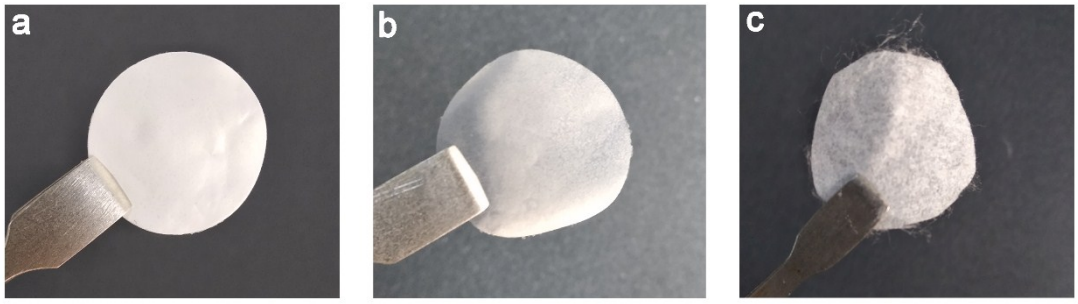

Fig. S7 Digital photographs of (a) the PA layer with the thickness of 40 μm, (b) the PA-HCOOH membrane, and (c) the pristine PA nonwoven material.

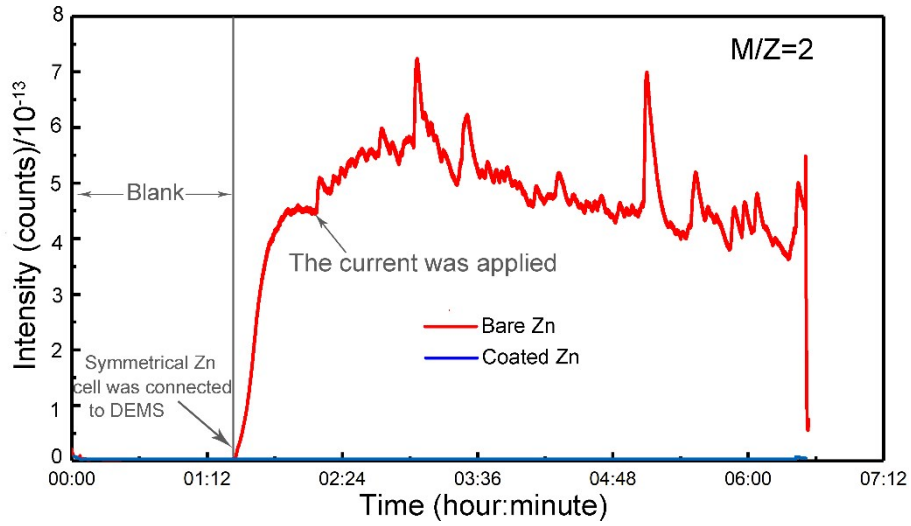

Fig. S8 Online DEMS data for symmetrical Zn batteries with the bare Zn and the coated Zn, respectively. Before being connected to the DEMS, the cells experienced a prolonged standing of 85 mins to check the chemical H_2 evolution. Then a current of 0.5 mA cm^{-2} was applied to charge/discharge for 6 cycles with each cycle time of 20 mins.

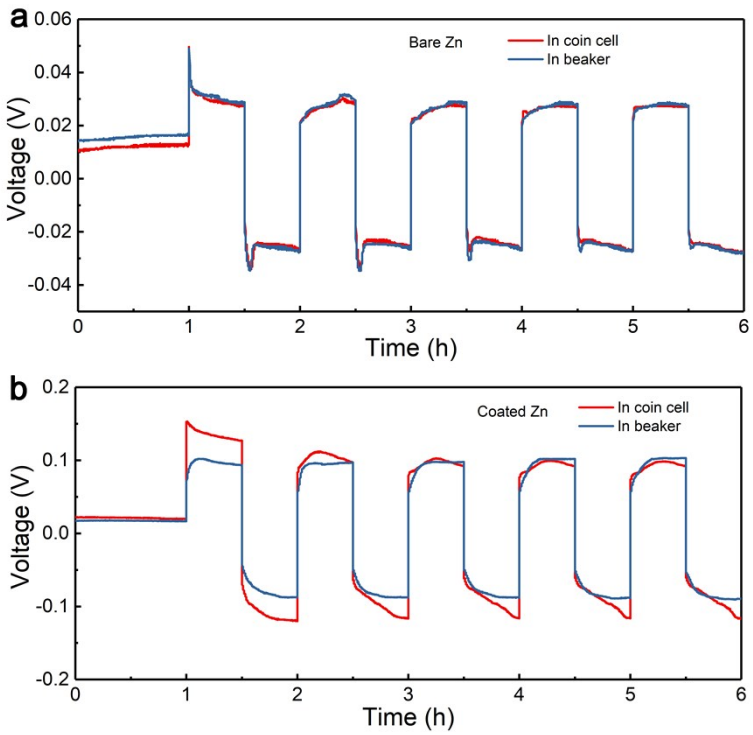

Fig. S9 (a) The initial five detailed voltage profiles of symmetrical cells with bare Zn in various configurations. (b) The initial five detailed voltage profiles of symmetrical cells with coated Zn in various configurations.

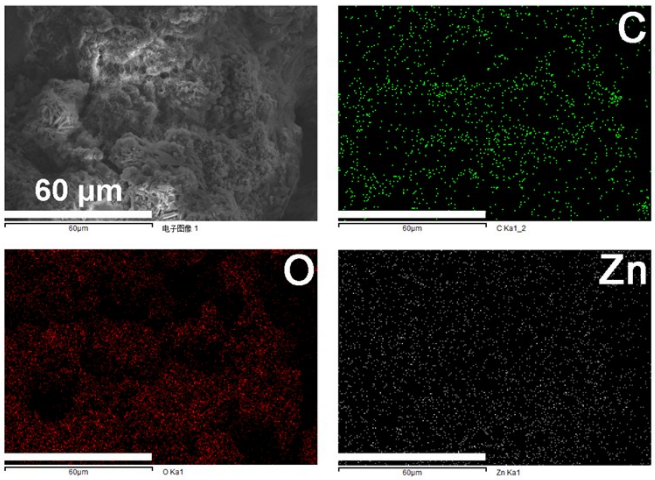

Fig. S10 SEM image and corresponding EDS analysis of the bare Zn after cycling 100 times in the transparent symmetrical Zn cell.

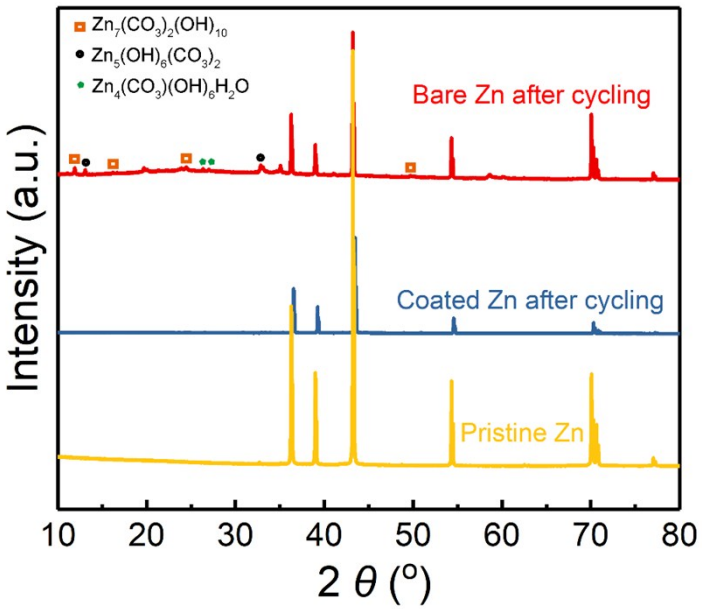

Fig. S11 XRD data of pristine Zn plate, coated Zn plate and bare Zn plate after cycling 100 times in the transparent symmetrical Zn cell.

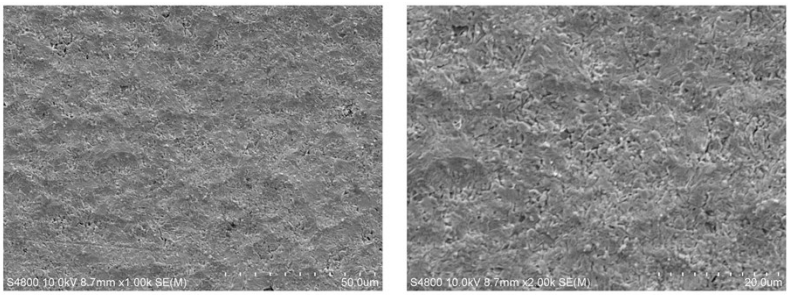

Fig. S12 SEM images of Zn deposition on coated Ti foil. (The PA layer was dissolved by cresol)

We have checked other solvents including methyl alcohol, N, N-dimethylformamide, phenol and cresol, which can possibly dissolve the PA. It turns out that only cresol can dissolve the PA layer by taking a long time. The Zn surface after being disposed by cresol exhibits a similar morphology with that being peeled off by tweezer (Fig. 4e), suggesting that the Zn surface was not destroyed by tearing off the PA layer.

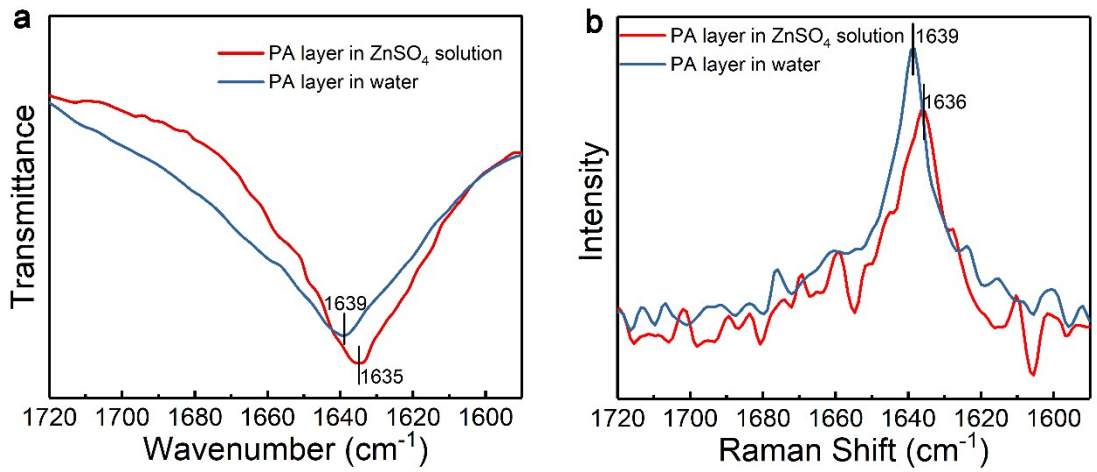

Fig. S13 (a) Fourier transform infrared spectra and (b) Raman spectra of the PA layer after being immersed in $ZnSO_4$ solution and pure water for 24 hours, respectively. The spectra were shown in the range of 1590 – 1720 cm^{-1} to indicate the variation of C=O.

The frequency of 1639 cm^{-1} derived from amide I mode (dominated by C=O stretching band) is shifted by ~4 cm^{-1} to a lower energy, indicating that Zn^{2+} ions or partially hydrated Zn^{2+} ions in the solution might break out or go across the solvation-sheath to coordinate with the oxygen sites of C=O, since Zn^{2+} ions are strong electron acceptors.

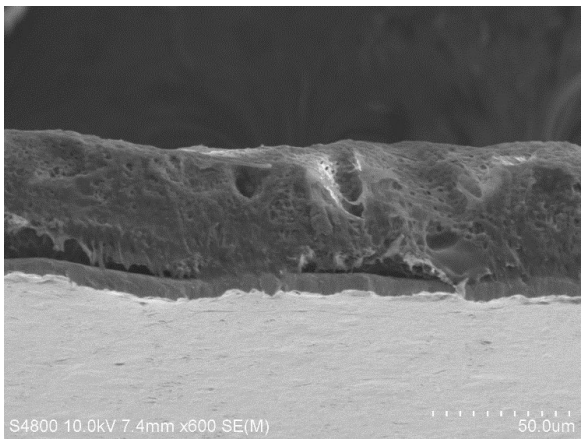

Fig. S14 The cross-sectional view of the coated Ti foil before electrodeposition.

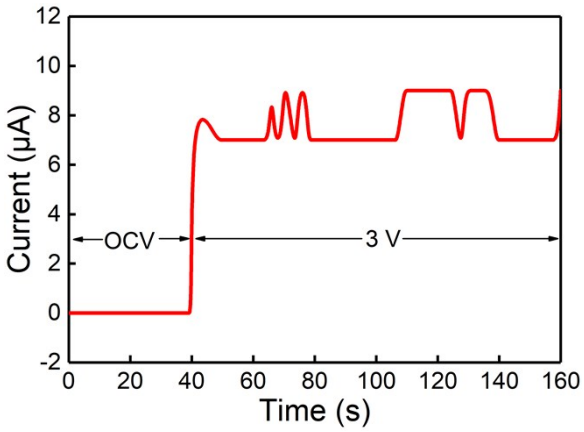

Fig. S15 The electronic conductivity test of the PA layer.

For electronic conductivity measurement of the PA layer, the current response to a step voltage of 3 V was measured. The PA-layer membranes were sandwiched between two stainless steel blocking electrodes. The electronic conductivity was calculated as following:

$$\sigma = \frac{L}{R \cdot S} = I \cdot \frac{L}{U \cdot S} \qquad \text{Equation (S4)}$$

where I is the average current responded, L is the thickness of the polymer film (40 μm in this work), U is the applied voltage, and S denotes the area of the contact between stainless steel and the film (2 cm^2 in this work).

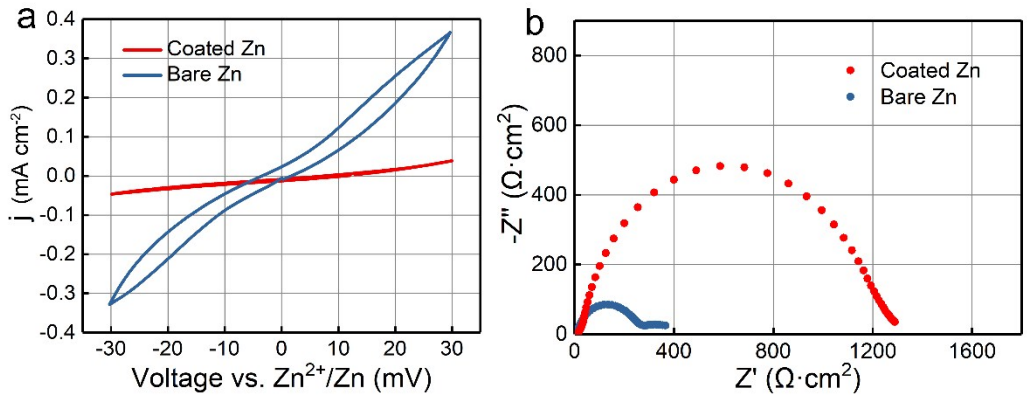

Fig. S16 (a) Polarization curves of bare Zn and coated Zn electrodes recorded with 1 mV s^{-1} scan rate and (b) impedance spectra of the bare Zn and coated Zn electrodes in 2 M $ZnSO_4$ electrolyte. Three-electrode cells were used for these tests using a Zn metal reference electrode and a Pt counter electrode.

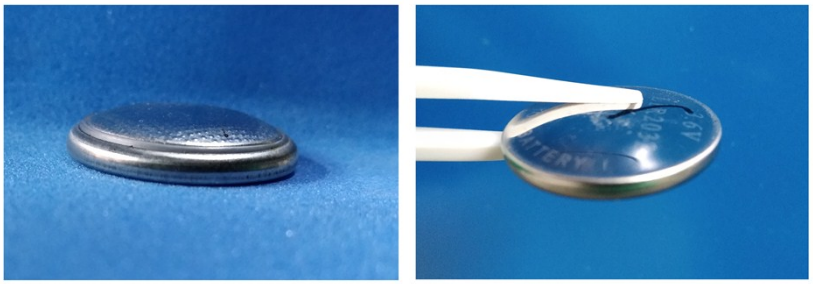

Fig. S17 The battery based on bare Zn exhibit an apparent volume expansion after cycling.

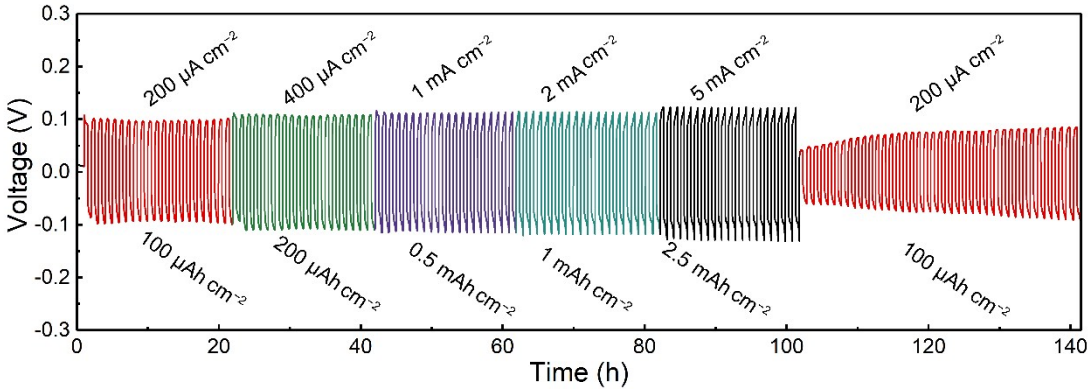

Fig. S18 Cycling performance of symmetrical Zn cell with coated Zn plates at varied current densities.

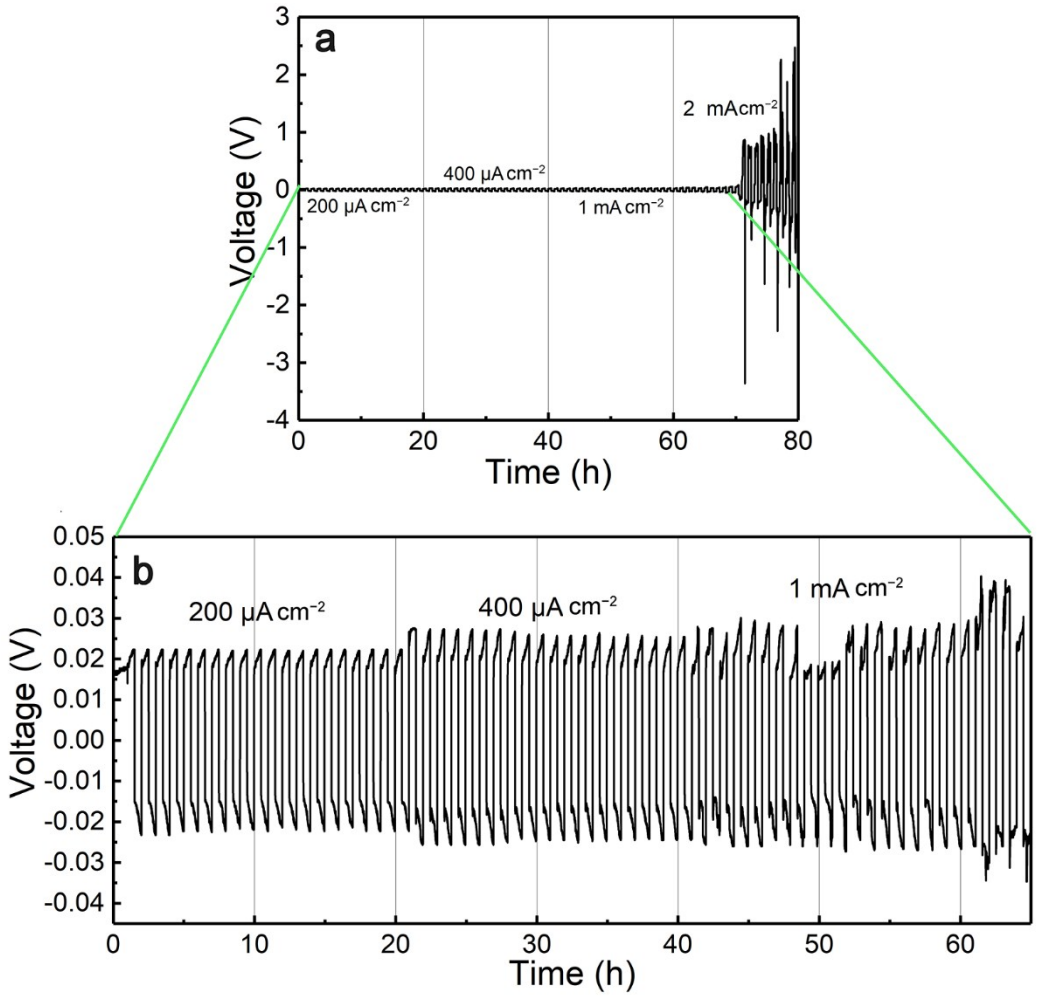

Fig. S19 (a) Cycling performance of symmetrical Zn cell with bare Zn plates at varied current densities and (b) its enlarged view from 0 to 65 hours.

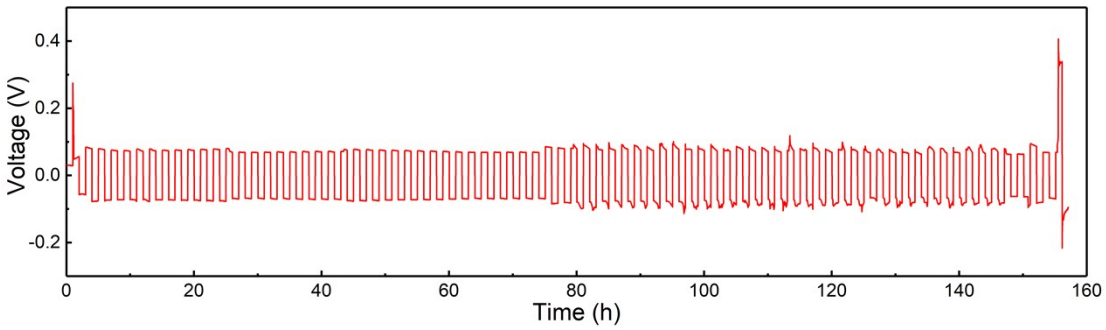

Fig. S20 Cycling performance of symmetrical Zn cell with coated Zn foils at an ultrahigh current density of 10 mA cm^{-2} and an areal capacity of 10 mAh cm^{-2}.

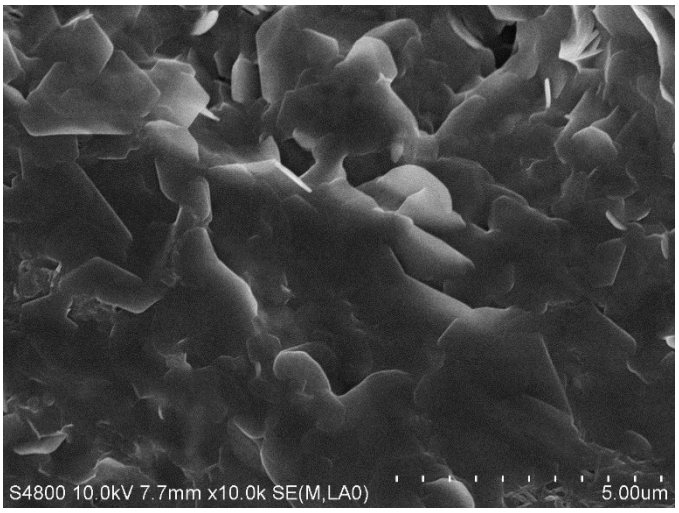

Fig. S21 SEM image of the surface of the coated Zn foil after being cycled at a current density of 10 mA cm^{-2} and an areal capacity of 10 mAh cm^{-2} (The PA layer was teared off).

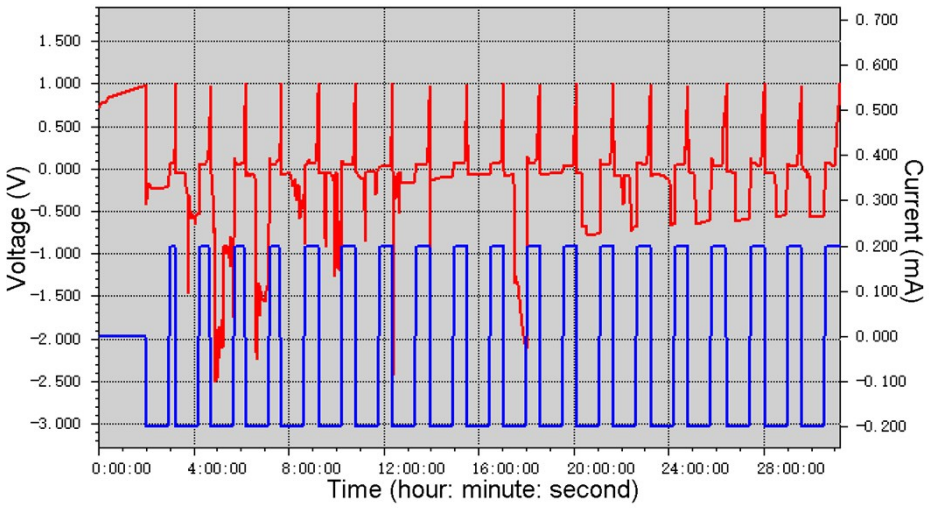

Fig. S22 Raw data from Land (Chinese version) for cycling test of Zn||Ti cell with the bare Ti electrode at a current density of 0.4 mA cm^{-2} (the area of Ti is 0.5 cm^2).

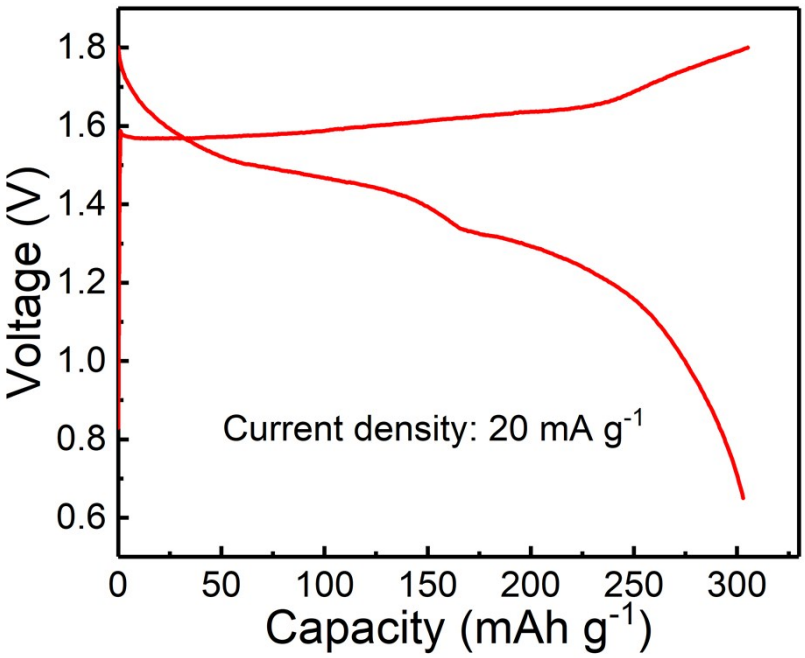

Fig. S23 Galvanostatic discharge-charge test of the coated Zn/MnO_2 cell at a minor current density of 20 mA g^{-1}. (second cycle, the cut-off charge voltage was set as 1.8 V to obtain the maximum capacity).

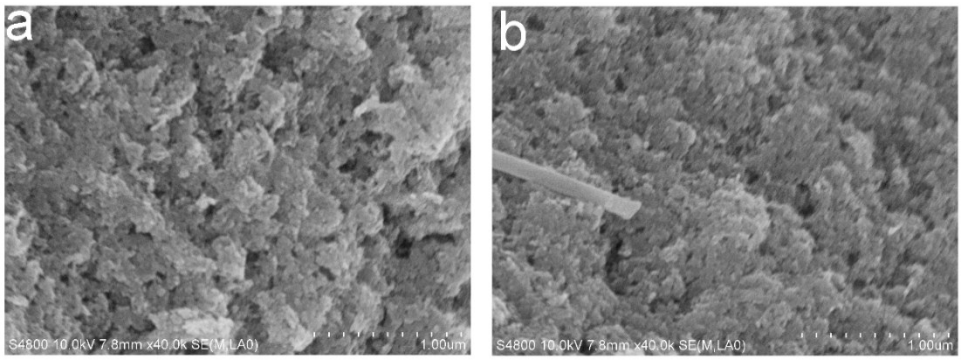

Fig. S24 Typical SEM images of MnO_2 after cycling in (a) bare Zn plate/MnO_2 battery and (b) coated Zn plate/MnO_2 battery.

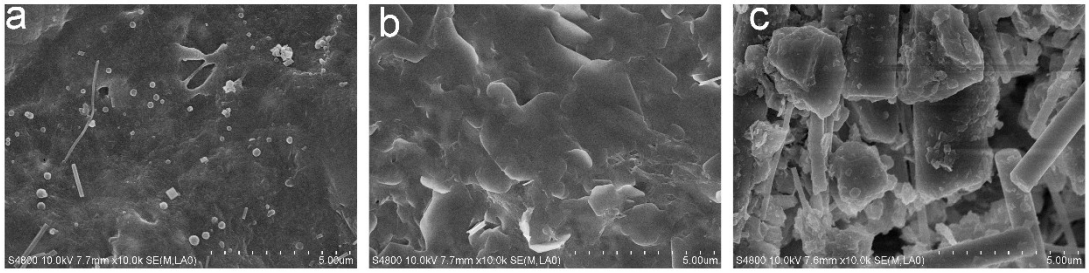

Fig. S25 (a) SEM images of the coated Zn plate anode after 1000 cycles in coated Zn/MnO_2 battery without further dispose, and (b) its corresponding surface in a higher magnification after tearing off the PA layer. (c) SEM image of the bare Zn plate anode in a higher magnification after cycling 450 times in bare Zn/MnO_2 battery.

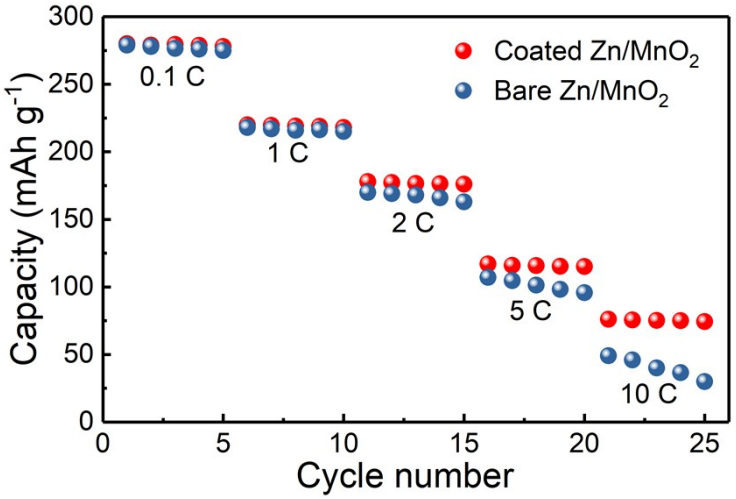

Fig. S26 Rate capability of the Zn/MnO_2 battery with bare Zn plate and coated Zn plate.

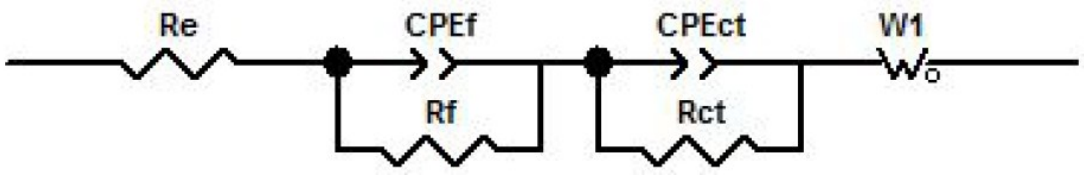

Fig. S27 The equivalent circuit used for fitting the experimental EIS data.

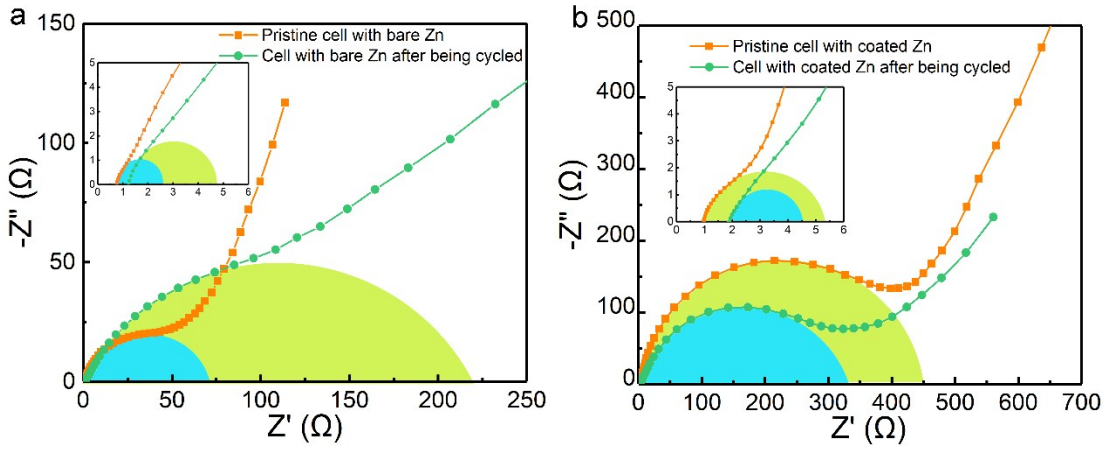

Fig. S28 EIS Nyquist plots of the Zn/MnO_2 batteries with (a) bare Zn anode and (b) coated Zn anode before and after cycling, respectively.

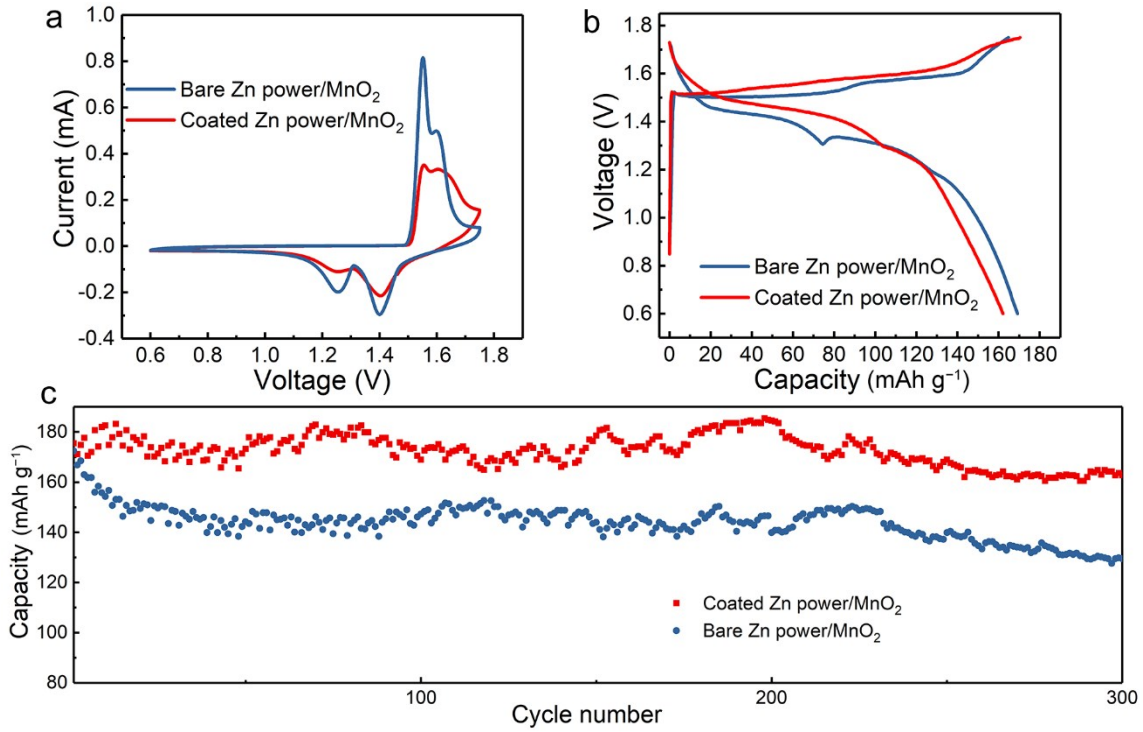

Fig. S29 Electrochemical performance of Zn/MnO_2 batteries based on Zn-power anode coated with PA layer in 2 M $ZnSO_4$ + 0.1 M $MnSO_4$. (a) Comparison of CV scanning (0.1mV s^{-1}, second cycle). (b) Galvanostatic charge/discharge curves at a current density of 2 C (second cycle). (c) Cycling performance at a current density of 2 C.

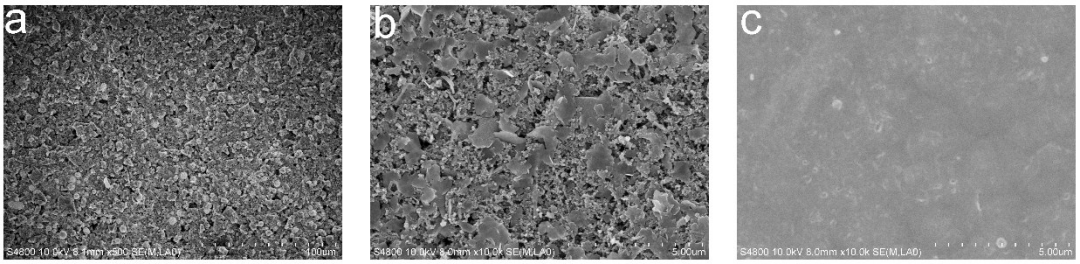

Fig. S30 SEM images of (a) pristine bare Zn-power anode, (b) bare Zn-power anode after 300 cycles, and (c) Zn-power anode coated with PA layer after cycling 300 times.

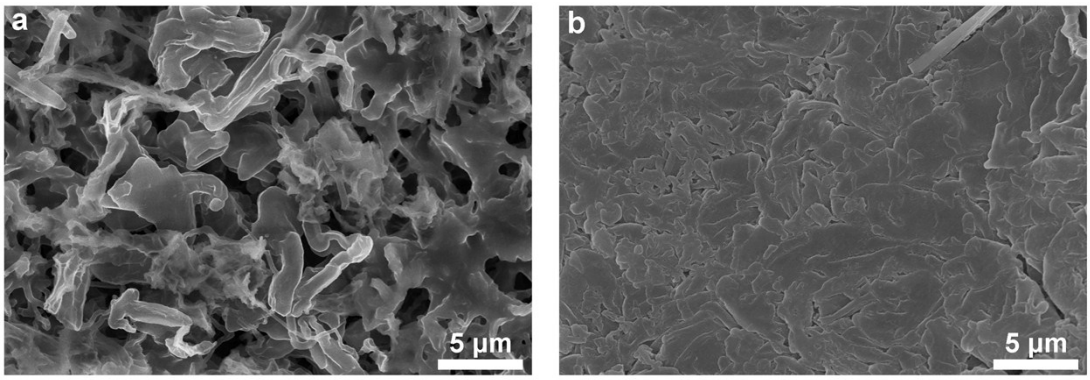

Fig. S31 SEM images of Li deposition on bare Cu foil (a) and coated Cu foil (b) at a current density of 0.3 mA cm^{-2} and an areal capacity of 3 mAh cm^{-2}. The PA layer was prepared in the same procedure that applied on Zn, but 2.5g bis(trifluoromethane)sulfonimide lithium (LiTFSI) was used instead of $Zn(TfO)_2$. 1 M $LiPF_6$-EC/DMC (ethylene carbonate/dimethyl carbonate) was employed as the electrolyte. The electrodes after being deposited were immersed in 1, 2-dimethoxyethane (DME) for 24 hours for swelling up the PA layer which was subsequently teared off.

Here we further engineered the PA layer on Cu substrate to check its role for regulating Li deposition. It is clear from Fig. S31a that the deposited Li on bare Cu features a porous and mussy structure, in accordance with previous observations.[2,3] By comparison, the deposited Li on coated Cu exhibits a dense and dendrite-free surface (Fig. S31b), which should be ascribed to the same manipulation of the nucleation process endowed by the PA interphase.

Table S1 Ionic conductivity and Zn^{2+} transference number of the 2 M $ZnSO_4$ aqueous electrolyte with various separators

Separator	GF	AGM	PE	No separator
Ionic conductivity (mS cm^{-1})	15.9	9.9	6.1	18.7
Zn^{2+} transference number	0.382	0.378	0.375	0.391

Table S2 Statistical results from DSC curves

Sample	T_g (°C)	T_{pm1} (°C, Main peak)	T_{pm2} (°C, Side peak)	X_{cr} (%)
Pristine PA	—	219.8	213.1	27.2
PA-HCOOH membrane	—	219.8	213.0	27.3
PA layer	-10	218.3	210.6	16.2

Degree of crystallinity was calculated according to Equation (S3) using the enthalpy of 100% crystalline material $\Delta H_{100\%cr}$ [kJ kg^{-1}] as reference. For the present work the value $\Delta H_{100\%cr}$ was considered equal to 230 kJ kg^{-1}.

$$X_{cr} = \Delta H / \Delta H_{100\%cr} \qquad \text{Equation (S5)}$$

where ΔH is the sample enthalpy in kJ kg^{-1} calculated as the area under the thermogram.

Table S3 Statistical results corresponding to Fig. S28

	R_{sf} (pristine/cycled)	R_{ct} (pristine/cycled)
Bare Zn anode	1.8/3.5 Ω	70/220 Ω
Coated Zn anode	4.4/2.7 Ω	450/328 Ω

Table S4 Comparison of electrochemical properties of the reported Zn anode after being optimized in various electrolytes

Modified strategies	Cycling performance of symmetrical Zn battery	The largest current density applied in the reference work	The largest areal capacity applied in the reference work	Ref.
3 M $Zn(CF_3SO_3)_2$ aqueous electrolyte	800 h (0.1 mA cm^{-2}, 0.1 mAh cm^{-2})	3.6 mA cm^{-2}	1 mAh cm^{-2}	4
$ZnSO_4$ solution with Na_2SO_4 additive	Not mentioned	8 mA cm^{-2}	0.76 mAh cm^{-2}	5
Highly concentrated aqueous electrolytes	170 h (0.2 mA cm^{-2}, 0.034 mAh cm^{-2})	Cannot be determined	2.4 mAh cm^{-2}	6
$ZnCl_2$ and acetamide eutectic solvent	150 h (0.2 mA cm^{-2}, 0.5 mAh cm^{-2})	0.2 mA cm^{-2}	0.5 mAh cm^{-2}	7
LiTFSI, $Zn(TFSI)_2$ and urea eutectic solvent	2400 h (0.1 mA cm^{-2}, 0.074 mAh cm^{-2})	1.48 mA cm^{-2}	2 mAh cm^{-2}	8
Ionic liquids ($[C_2mim][dca]$ + 3 wt% H_2O + 9 mol% $Zn(dca)_2$)	380 h (0.2 mA cm^{-2}, 0.4 mAh cm^{-2})	0.5 mA cm^{-2}	1 mAh cm^{-2}	9
Ionic liquid containing nickel triflate	Not mentioned	0.2 mA cm^{-2}	0.2 mAh cm^{-2}	10
Acetamide and zinc perchlorate binary molten electrolyte	Not mentioned	0.1 mA cm^{-2}	0.855 mAh cm^{-2}	11

Organic electrolyte based on triethyl phosphate (TEP) solvent	200 h (1 mA cm^{-2}, 1 mAh cm^{-2})	1 mA cm^{-2}	5 mAh cm^{-2}	12
PVA/$Zn(CF_3SO_3)_2$ hydrogel electrolyte	800 h (0.1 mA cm^{-2}, 0.1 mAh cm^{-2})	3 mA cm^{-2}	0.123 mAh cm^{-2}	13
PVdF-HFP based polymer electrolytes	Not mentioned	1 mA cm^{-2}	Cannot be determined	14
PAM-based hierarchical polymer electrolyte	Not mentioned	6.93 mA cm^{-2}	0.765 mAh cm^{-2}	15
A MOF-based single-ion Zn^{2+} solid electrolyte	360 h (0.1 mA cm^{-2}, 0.05 mAh cm^{-2})	0.4 mA cm^{-2}	0.25 mAh cm^{-2}	16
PAN-based cation exchange membrane	350 h (0.5 mA cm^{-2}, 0.25 mAh cm^{-2})	2 mA cm^{-2}	1 mAh cm^{-2}	17
Nano-$CaCO_3$ coating	836 h (0.25 mA cm^{-2}, 0.05 mAh cm^{-2})	3 mA cm^{-2}	0.1 mAh cm^{-2}	18
TiO_2 coating	Over 150 h (1 mA cm^{-2}, 1 mAh cm^{-2})	3 mA cm^{-2}	1 mAh cm^{-2}	19
Regulate Zn anodes by multifunctional polymer interphase	***Over 8000 h (0.5 mA cm^{-2}, 0.25 mAh cm^{-2})***	***10 mA cm^{-2}***	***10 mAh cm^{-2}***	***This work***

The cycling performmance of symmetrical Zn battery can sufficiently characterize the reversibility of the Zn anode, which is a common sense. The largest current density and areal capacity that applied in the anode can effectively indicate the possibility for

practical applications. Accordingly, we list the cycling performmance of symmetrical Zn battery, the largest current density and the largest areal capacity, involved in the latest woks, to demonstrate the recent advances in the state-of-the-art two-dimension Zn anode. It should be noted that it is unfair to compare the density current and areal capacity between the planar and three-dimension Zn anode given the large active area in three-demension construction, therefore the three-demension works such as nanorod and nanowire were neglected.

Reference:

1. H. Pan, Y. Shao, P. Yan, Y. Cheng, K. S. Han, Z. Nie, C. Wang, J. Yang, X. Li and P. Bhattacharya, Nature Energy, 2016, 1, 16039.
2. G. Zheng, C. Wang, A. Pei, J. Lopez, F. Shi, Z. Chen, A. D. Sendek, H.-W. Lee, Z. Lu and H. Schneider, ACS Energy Lett., 2016, 1, 1247.
3. S. Li, L. Fan and Y. Lu, Energy Storage Mater., 2019, 18, 205
4. N. Zhang, F. Cheng, Y. Liu, Q. Zhao, K. Lei, C. Chen, X. Liu and J. Chen, *J. Am. Chem. Soc.*, 2016, **138**, 12894.
5. F. Wan, L. Zhang, X. Dai, X. Wang, Z. Niu and J. Chen, *Nat. Commun.*, 2018, **9,** 1656.
6. F. Wang, O. Borodin, T. Gao, X. Fan, W. Sun, F. Han, A. Faraone, J. A. Dura, K. Xu and C. Wang, *Nat. Mater.*, 2018, **17**, 543.
7. Y. Wang, Z. Niu, Q. Zheng, C. Zhang, J. Ye, G. Dai, Y. Zhao and X. Zhang, *Sci. Rep.*, 2018, **8**, 5740.
8. J. Zhao, J. Zhang, W. Yang, B. Chen, Z. Zhao, H. Qiu, S. Dong, X. Zhou, G. Cui and L. Chen, *Nano Energy*, 2019, **57**, 625.
9. T. J. Simons, D. R. MacFarlane, M. Forsyth and P. C. Howlett, *ChemElectroChem*, 2014, **1**, 1688.
10. Z. Liu, T. Cui, G. Pulletikurthi, A. Lahiri, T. Carstens, M. Olschewski and F. Endres, *Angew. Chem. Int. Ed.*, 2016, **55**, 2889.
11. N. V. Narayanan, B. Ashokraj and S. Sampath, *J. Colloid Interface Sci.*, 2010, **342**, 505.

12. A. Naveed, H. Yang, J. Yang, Y. Nuli and J. Wang, *Angew. Chem. Int. Ed.*, 2019, **58**, 2760.

13. S. Huang, F. Wan, S. Bi, J. Zhu, Z. Niu, and J. Chen, *Angew. Chem. Int. Ed.*, 2019, **58**, 4313.

14. J. P. T. Guisao and A. J. F. Romero, *Electrochim. Acta*, 2015, **176**, 1447.

15. H. Li, C. Han, Y. Huang, Y. Huang, M. Zhu, Z. Pei, Q. Xue, Z. Wang, Z. Liu and Z. Tang, *Energy Environ. Sci.*, 2018, **11**, 941.

16. Z. Wang, J. Hu, L. Han, Z. Wang, H. Wang, Q. Zhao, J. Liu and F. Pan, *Nano Energy*, 2019, **56**, 92.

17. B.-S. Lee, S. Cui, X. Xing, H. Liu, X. Yue, V. Petrova, H.-D. Lim, R. Chen and P. Liu, *ACS Appl. Mater. Interfaces*, 2018, **10**, 38928.

18. L. Kang, M. Cui, F. Jiang, Y. Gao, H. Luo, J. Liu, W. Liang and C. Zhi, *Adv. Energy Mater.*, 2018, **8**, 1801090.

19. K. Zhao, C. Wang, Y. Yu, M. Yan, Q. Wei, P. He, Y. Dong, Z. Zhang, X. Wang and L. Mai, *Adv. Mater. Interfaces*, 2018, **5**, 1800848.